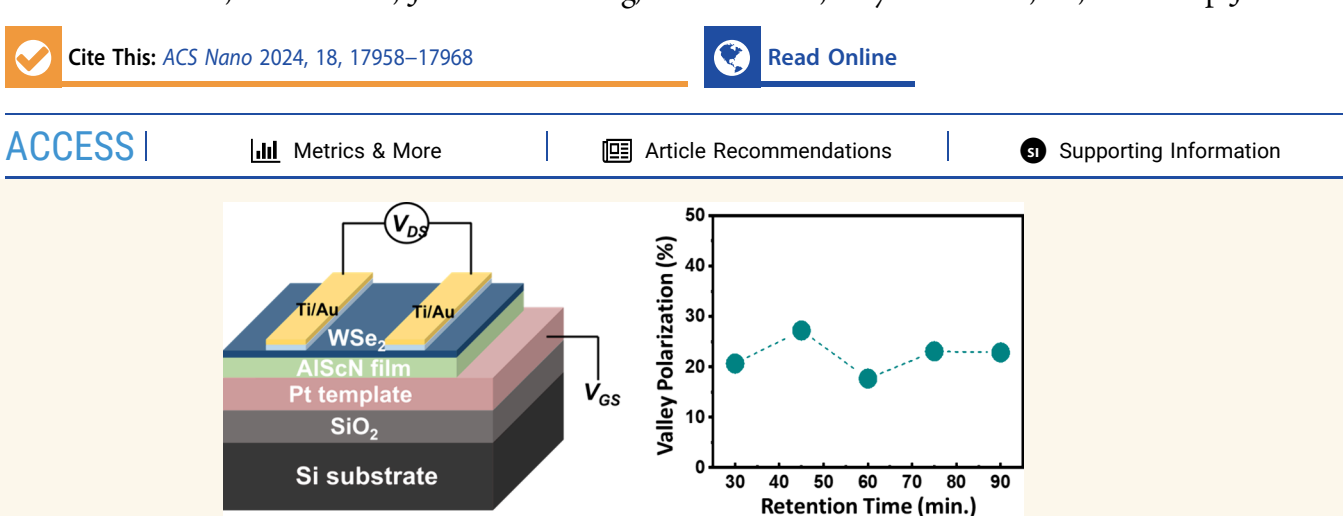


www.acsnano.org

Nonvolatile Control of Valley Polarized Emission in 2D WSe₂-AlScN Heterostructures

Simrjit Singh, Kwan-Ho Kim, Kiyoung Jo, Pariasadat Musavigharavi, Bumho Kim, Jeffrey Zheng, Nicholas Trainor, Chen Chen, Joan M. Redwing, Eric A. Stach, Roy H. Olsson, III, and Deep Jariwala*



ABSTRACT: Achieving robust and electrically controlled valley polarization in monolayer transition metal dichalcogenides (ML-TMDs) is a frontier challenge for realistic valleytronic applications. Theoretical investigations show that the integration of 2D materials with ferroelectrics is a promising strategy; however, an experimental demonstration has remained elusive. Here, we fabricate ferroelectric field-effect transistors using a ML-WSe₂ channel and an $Al_{0.68}Sc_{0.32}N$ (AlScN) ferroelectric dielectric and experimentally demonstrate efficient tuning as well as non-volatile control of valley polarization. We measure a large array of transistors and obtain a maximum valley polarization of ~27% at 80 K with stable retention up to 5400 s. The enhancement in the valley polarization is ascribed to the efficient exciton-to-trion (X-T) conversion and its coupling with an out-of-plane electric field, viz., the quantum-confined Stark effect. This changes the valley depolarization pathway from strong exchange interactions to slow spin-flip intervalley scattering. Our research demonstrates a promising approach for achieving non-volatile control over valley polarization for practical valleytronic device applications.

KEYWORDS: WSe2, ferroelectric, valley-polarization, non-volatile, nitrides

INTRODUCTION

Valleytronics is an emerging field whereby, the electron's valley degree of freedom (DoF), rather than its charge, is exploited to store and process binary information. 1,2 Two-dimensional transition metal dichalcogenides (2D-TMDs) possess two inequivalent valleys in momentum space at the K and K' points in the first hexagonal Brillouin zone. This makes them particularly attractive for exploiting valleytronic phenomena.^{2,3} The strong spin-valley locking effect gives rise to valleydependent optical selection rules, enabling selective control of carriers in the K and K' valleys using circularly polarized light of different helicity.4 Furthermore, a large momentum separation between the two valleys is expected to lead to a slow decay of the valley information. Owing to these fascinating properties, a variety of valley-contrasting phenomena such as the valley selective circular dichroism, 5,6 the optical Stark effect,^{7–9} the valley Hall effect,^{10,11} the valley Zeeman

effect, ^{12,13} etc. have been successfully demonstrated by using various 2D-TMD systems. In spite of these significant advancements, the development of highly tunable valleytronic devices, analogous to solid-state microelectronics, is required to make valleytronics a viable commercial technology.

In valleytronic devices that rely upon the optical manipulation of valleys, the degree of valley polarization and the lifetime of valley polarized states are critical measures. The valley lifetime of excitons in monolayer TMDs (ML-TMDs) is typically quite low, owing to strong electron—hole exchange

Received: April 9, 2024 Revised: June 5, 2024 Accepted: June 12, 2024 Published: June 26, 2024





interactions, leading to fast valley depolarization. ^{14,15} Additionally, the typical volatile nature of optically initialized valley polarization severely degrades the fidelity of the valley information. Alternative strategies, such as the magnetic proximity effect, have been used to obtain nonvolatile valley splitting in ML-TMDs. ^{16–18} However, the magnitude of valley splitting obtained was quite low (in the range of 0.1–0.2 meVT⁻¹). Further, the requirement of a high magnetic field increases the complexity and energy consumption of devices. Thus, it is important to look for alternative ways to achieve static and robust valley polarization for practical applications.

Electrical control of the valley DoF is highly desired for large-scale integration and energy-efficient tuning. The electrical control of valley pseudospin in ML-TMDs has not been well studied. Few reports use electrostatic gating in standard field effect transistors (FETs) to control valley polarization. 19–21 The gate-controlled exciton-to-trion (X-T) conversion has been shown to prolong the lifetime of valleypolarized charge carriers by suppressing the electron-hole exchange interaction strength and, consequently, intervalley scattering. Traditional electrostatic gating uses a linear dielectric material and relies on electric field adjustments and Fermi-level tuning in field effect transistor (FET) geometry. In addition, the effect of doping in linear dielectrics lasts only until the voltage is being applied. In comparison, the potential of non-volatile electrical control of valley polarization using nonlinear ferroelectric dielectrics has received limited investigation. This unexplored approach offers possibilities for valley manipulation and control in addition to realizing giant electric fields and electrostatic tunability in 2D-TMDs.

Ferroelectric materials possess a spontaneous polarization, originating from their noncentrosymmetric structure, which remains robust even when the applied gate voltage is removed. Moreover, the reversibility of ferroelectric polarization with the application of external electric fields could effectively enhance polarization-dependent functionalities of valleytronic devices. Several reports using first-principles calculations indicate that ferroelectric polarization switching is a potential knob to modulate valley pseudospin in various 2D materials. However, an experimental manifestation of this approach has yet to be demonstrated with stable nonvolatile programming.

Herein, we demonstrate ferroelectric field effect transistors (FeFETs) using mechanically exfoliated as well as MOCVDgrown WSe₂ monolayers transferred on top of Al_{0.68}Sc_{0.32}N (AlScN) dielectric that exhibit tunable, non-volatile, valleypolarized emission. AlScN is a recently discovered ferroelectric material displaying out-of-plane electrical polarization and superior ferroelectric properties, including very high remnant polarization (>115 μ C/cm²) and coercive fields (2–6 MV/ cm), compared to other commonly utilized ferroelectric materials. 26-32 This makes AlScN (and related ferroelectrics) very interesting not just from the perspective of practical ferroelectric memory applications but also from fundamental investigation since coupling them to 2D semiconductors where in large electric fields and carrier doping densities can be applied in a non-volatile manner to an ultrathin quantum confined layer. Taking advantage of the ferroelectric properties of AlScN, we investigate valley polarization characteristics of ML-WSe2 using ferroelectric polarization switching and demonstrate efficient tuning as well as non-volatile control of valley polarization. We measure a large array of FeFETs and observe a maximum degree of valley polarization (DVP) of

~27% with stable retention up to 5400 s at 80 K. The robust control of valley polarization was ascribed to the formation of charged excitons and their coupling with a large out-of-plane electric field associated with the large ferroelectric polarization of AlScN, leading to suppressed electron—hole exchange interactions and, thereby, suppressed intervalley scattering. Our results provide a promising integration strategy for non-volatile electrical control of valley properties in ML-TMDs for polarization tunable emitters.

RESULTS AND DISCUSSION

The prototypical FeFET in this study consists of monolayer WSe₂ as a semiconductor channel on top of a 45 nm thick AlScN ferroelectric dielectric film grown on a $Pt(111)/Ti/SiO_2/Si$ substrate. A schematic of the device structure is shown in Figure 1a. The Ti/Au metal electrodes are used as the

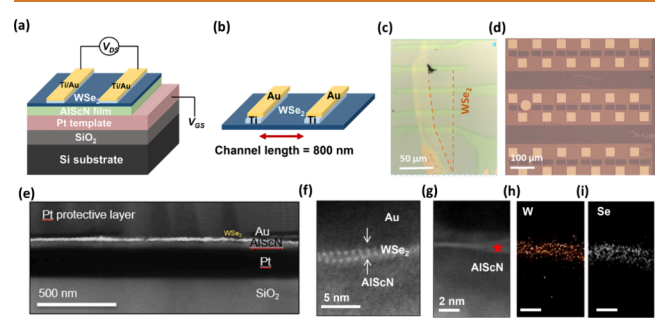


Figure 1. WSe₂/AlScN valleytronic device structure. (a, b) Schematic representation of the WSe₂/AlScN FeFET device. The Ti–Au metals are used as the source/drain electrodes, and the Pt layer is used as the bottom gate electrode. The channel length in the device is \sim 800 nm. (c) Optical image of the devices fabricated using mechanically exfoliated WSe₂ monolayers. (d) Optical image of a large array of the devices fabricated from the large area mechanically exfoliated monolayers using our modified exfoliation method. (e) Cross-sectional BFTEM image of a representative WSe₂/AlScN device showing different material layers in the device. (f) Atomically resolved STEM image of the WSe₂/AlScN interface, which clearly shows a monolayer thickness of WSe₂. (g–i) Energy-dispersive X-ray spectroscopic image of the W and Se in the monolayer WSe₂.

source and drain, and a conductive Pt layer is used as the bottom gate electrode. The channel length in the device is kept at ~800 nm (Figure 1b). The devices were fabricated using both mechanically exfoliated WSe₂ (μ m² to cm² scale monolayers, using our modified exfoliation technique) as well as MOCVD-grown WSe2 monolayers (See Methods and Experimental Section for details). A large array of the devices is also fabricated from both mechanically exfoliated and MOCVD-grown cm²-scale WSe₂ monolayers. Optical images of representative devices are shown in Figure 1c,d. Figures S1-S3, in the Supporting Information, display photoluminescence (PL) intensity maps, an atomic force microscopy (AFM) image, and Raman spectra for monolayer WSe2 samples used in this study. The interfacial characteristics of a representative WSe₂/AlScN FeFET device are also imaged by using bright field cross-sectional transmission electron microscopy (BFTEM), as shown in Figure 1e. The high-angle annular dark field scanning transmission electron microscopy (STEM) image of the WSe₂/AlScN interface combined with elemental analysis (Figure 1f-i) shows a monolayer of WSe₂ on top of

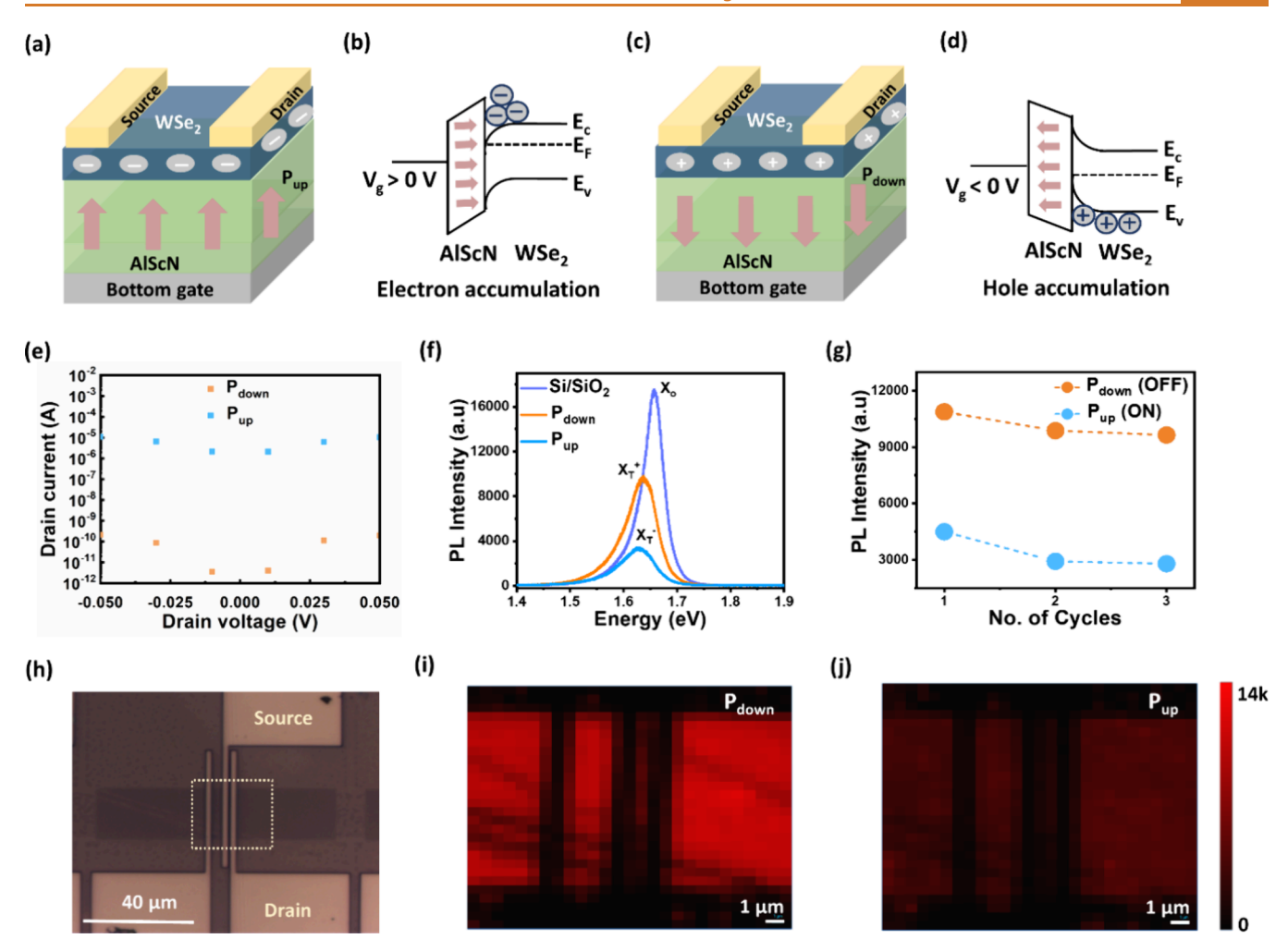


Figure 2. Ferroelectric polarization switching in the WSe₂/AlScN FeFET device; electrical and optical characteristics of the device. (a–d) Schematic illustration of ferroelectric polarization switching, i.e., (a) upward, $P_{\rm up}$ and (c) downward, $P_{\rm down}$ polarized states in the WSe₂/AlScN FeFET device. (b and d) The corresponding energy band alignment between the WSe₂ and AlScN in $P_{\rm up}$ and $P_{\rm down}$ states. The positive gate bias switches the ferroelectric polarization upward, resulting in the accumulation of electrons in the WSe₂ channel (b). The negative gate bias switches the ferroelectric polarization downward, resulting in hole accumulation in the WSe₂ channel (d). (e) The polarization switching is confirmed from the room temperature $I_{\rm d}$ – $V_{\rm d}$ curves at $V_{\rm g}$ of 0 V of the WSe₂/AlScN FeFET device in two oppositely polarized states. (f) PL spectra of WSe₂ transferred on Si/SiO₂, $P_{\rm up}$ and $P_{\rm down}$ polarized AlScN substrate. (g) Modulation of PL emission intensity in the $P_{\rm up}$ and $P_{\rm down}$ states for multiple cycles of the ferroelectric polarization switching. (h–j) The corresponding PL intensity maps of the WSe₂/AlScN FeFET device in the $P_{\rm down}$ and $P_{\rm up}$ states shows significant quenching of PL emission in the $P_{\rm up}$ state.

AlScN. There is no evidence of a significant oxide layer between WSe₂ and AlScN.

Ferroelectric polarization switching in the WSe₂/AlScN FeFET device is accomplished by the application of a gate bias $(V_{\rm g})$. When a positive $V_{\rm g}$ is applied, the electric dipoles in the ferroelectric-AlScN layer are polarized upward $(P_{\rm up})$, pointing toward the channel (Figure 2a). As a result, the energy band alignment between AlScN and WSe2 is tuned by the presence of an applied electric field. The conduction band of WSe2 is bent below the Fermi level (E_F) , resulting in the accumulation of mobile electrons in the WSe₂ channel (Figure 2b) and an accompanying increase in the channel conduction, as confirmed by the I_d - V_d curves (Figure 2e) (See linear scale I_d-V_d characteristics of representative devices in Supporting Information Figure S11). A sharp increase in the drain current in the P_{up} state confirmed the accumulation of an excess of electrons in the WSe2 channel. We estimate the carrier concentration of the WSe_2 device in the P_{up} state from the transfer curves presented in Figure S11 (see Supporting

Information), which was found to be $\sim 3.3 \times 10^{12}$ cm⁻². In contrast, when a negative " $V_{\rm g}$ " is applied, AlScN is polarized downward (P_{down}) (Figure 2c). In this case, the valence band is bent above the $E_{\rm F}$, and an excess of hole density is accumulated in WSe2 (Figure 2d), resulting in a decrease in the channel conductance (Figure 2e) (See I_d – V_g characteristics of representative devices in Supporting Information Figure S11). Importantly, the ferroelectric polarization maintains the channel state in the devices, even after the removal of the gate voltage, enabling non-volatile control of valley polarization. This is a conceptually interesting form of optoelectronic memory that can store information in both the electrical conductance of the semiconducting channel of the FeFET and the degree of circular polarization of the photoluminescence of the channel. Specifically, the $P_{\rm up}$ state can be described as the low resistance "ON" state, and the $P_{\rm down}$ state can be described as a high resistance "OFF" state. The presence of external charge carriers can strongly influence the PL characteristics of ML-TMDs: the photoexcited electrons and holes can combine

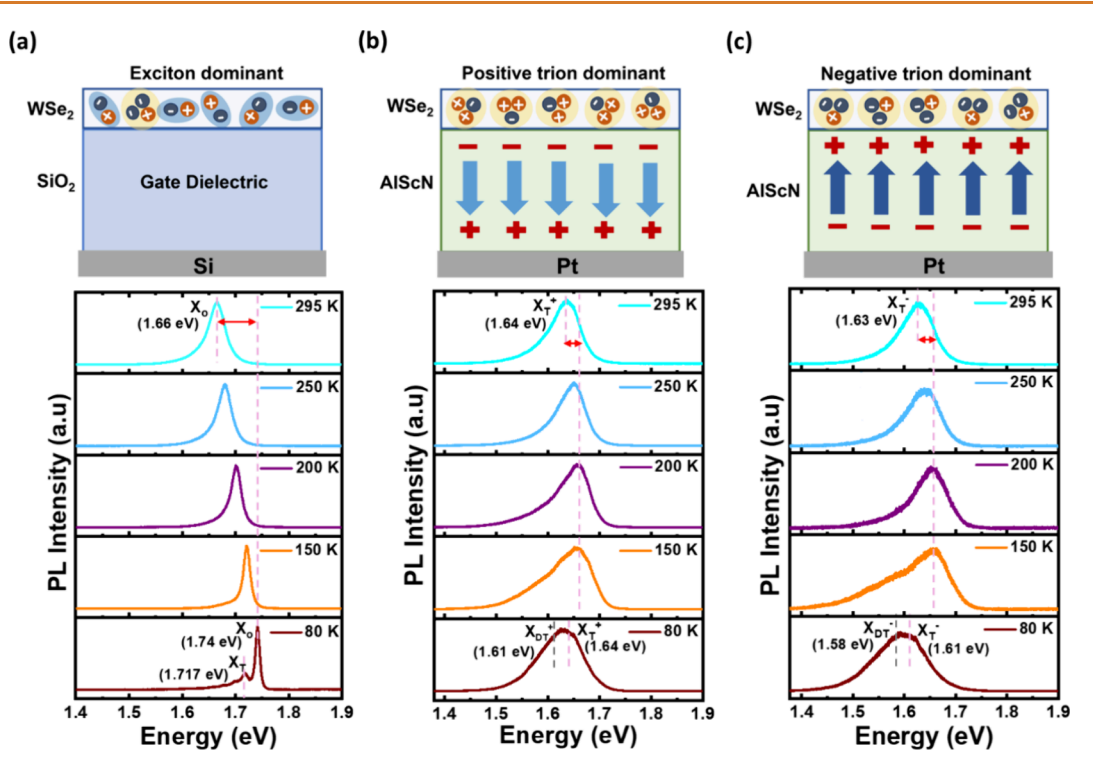


Figure 3. Temperature-dependent photoluminescence characteristics of monolayer WSe₂ exfoliated on (a) nonferroelectric SiO₂/Si substrate and (b) P_{down} polarized and (c) P_{up} polarized AlScN substrate. Top panels show dominant excitonic species in the devices. The WSe₂/SiO₂/Si device is exciton dominant whereas, in the P_{down} polarized, the positively charged trions dominate the WSe₂/AlScN FeFET device due to the accumulation of excess of holes in WSe₂. In the P_{up} polarized, the negatively charged trions dominate the WSe₂/AlScN device due to the accumulation of excess electrons in the WSe₂ monolayer.

with the extra charge carriers to form negatively or positively charged trions, even at room temperature. To determine the effect of ferroelectric polarization switching on the excitonic characteristics of WSe₂, we performed PL spectroscopy measurements on the devices when subjected to differently polarized states (Figure 2f). For ML-WSe₂ exfoliated onto a SiO₂/Si substrate, the PL spectra feature a highly intense emission from the neutral excitons (X°) due to the large radiative recombination of photogenerated electrons and holes. In contrast, the PL spectrum from the WSe₂/AlScN device in the $P_{\rm down}$ state was strongly suppressed and red-shifted to ~20 meV due to the formation of positively charged trions (X_T^+) in the hole-rich WSe₂. When the ferroelectric polarization direction is switched to the $P_{\rm up}$ state, a high density of negative charges injected in WSe₂ results in the formation of negatively charged trions (X_T^-) , leading to further suppression of the PL emission intensity and a red shift.^{33–35} The observed variation in PL intensities among neutral excitons, positive and negative trions can be attributed to the different binding energies as well as higher rates of nonradiative recombination of trions compared to neutral excitons, thereby influencing the energy required for carriers to recombine. We observed that this PL modulation is quite reversible and can be switched to the "ON" and "OFF" states for multiple cycles of ferroelectric polarization switching (Figure 2g).

To further verify the spatial homogeneity of the injected charge carriers with ferroelectric gating, we took PL intensity maps from the WSe₂/AlScN device in two oppositely polarized states (Figure 2h–j and Figure S4). It is evident from Figure 2i,j that the PL intensity is altered significantly over the region close to the metal electrodes when the polarization is switched from the $P_{\rm down}$ to the $P_{\rm up}$ state, implying an efficient

polarization switching and, importantly, that the switching is not limited to the area under the top metal electrodes only but spreads laterally up to a few μ ms away from the electrodes. The above features confirm that ferroelectric polarization-induced gating can effectively modulate the optical characteristics of monolayer WSe₂ over the entire channel region.

To obtain additional insight into the excitonic properties of WSe₂ resulting from ferroelectric gating, we performed temperature-dependent PL measurements. Figure 3a-c displays temperature-dependent (295 to 80 K) PL spectra from the ML-WSe₂ samples exfoliated on both SiO₂/Si and AlScN substrates in two oppositely polarized states, under 633 nm laser excitation. At room temperature, the PL spectrum from the WSe₂/SiO₂/Si device displays emission from the neutral intralayer excitons (X°) , which exhibits a gradual blue shift of ~80 meV with significant PL line width narrowing upon cooling to 80 K. This observation is in good agreement with previous reports from monolayer TMDs (Figure 3a). 36,37 At 80 K, a shoulder peak corresponding to the formation of trions is also observed due to unintentional doping in as-exfoliated monolayer WSe₂.³⁸ As shown in Figure 3b, the PL emission from the $WSe_2/AlScN$ FeFET device polarized in the P_{down} state is red-shifted to \sim 20 meV below the X° emission energy and exhibits significant PL broadening, possibly due to the modified dielectric environment. This can be ascribed to the formation of positively charged bright trions $(X_T^+)^{.39,40}$ As the temperature is decreased, $X_{\rm T}^{+}$ displays a blue shift of ~10 meV, which is significantly less than the shift observed for X° (~80 meV) in the WSe₂/SiO₂/Si device. Interestingly, at 80 K, a large red shift of ~110 meV with significant line width broadening in the X_T^+ PL peak relative to the PL peak position of neutral excitons was observed. The red shift in the PL peaks

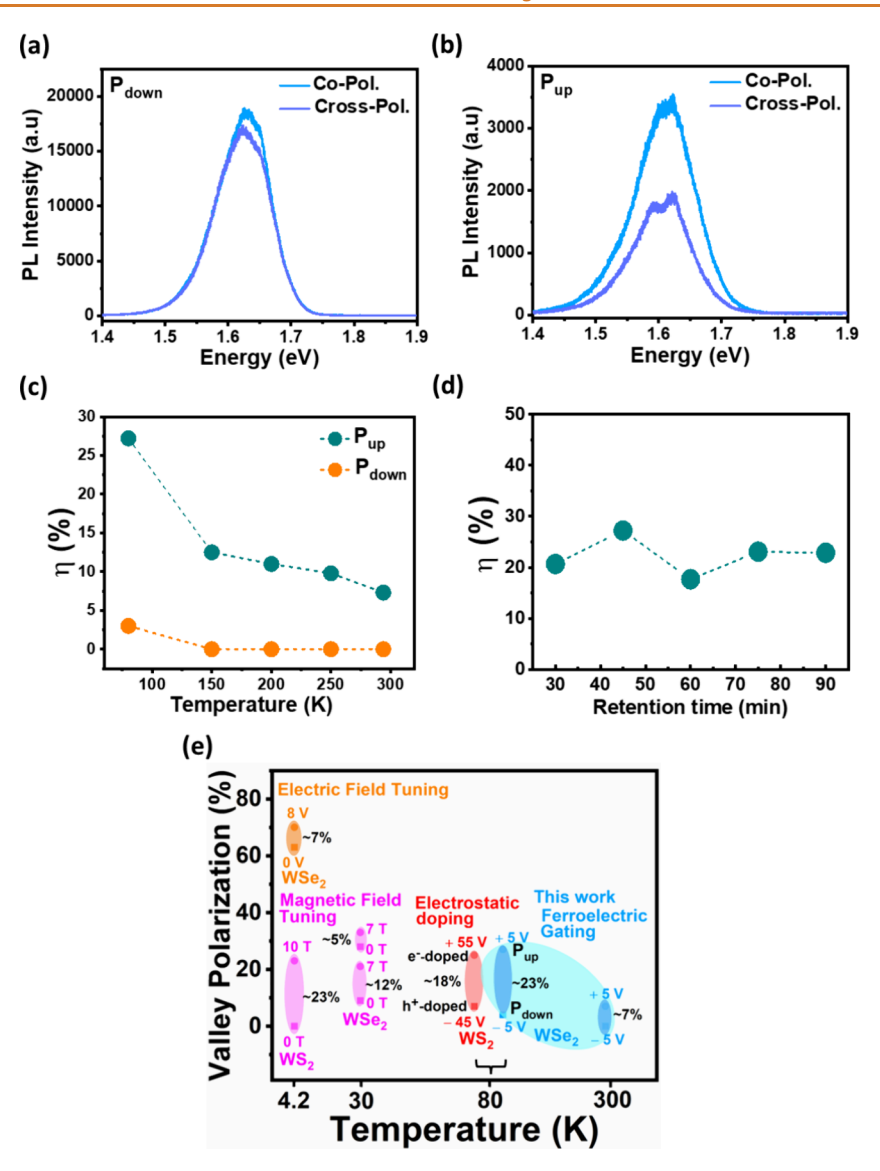


Figure 4. Valley polarization characteristics of WSe₂/AlScN FeFET devices. (a) Helicity resolved PL spectra from the WSe₂/AlScN device in $P_{\rm down}$ state. (b) Helicity resolved PL spectra from the WSe₂/AlScN device in $P_{\rm up}$ state, at 80 K. (c) Temperature-dependent valley polarization characteristics of the WSe₂/AlScN device in the $P_{\rm up}$ and $P_{\rm down}$ polarized states. (d) Retention characteristics of valley polarization in the $P_{\rm up}$ polarized WSe₂/AlScN device. (e) Comparison plot of previously reported values of valley polarization tuning in various monolayer TMD systems. The orange dots denote tuning with an electric field. Magenta dots denote tuning with a magnetic field. Red dots denote tuning with electrostatic doping, and blue dots denote tuning with ferroelectric polarization switching in our work. 19,20,47,48

can be ascribed to the quantum-confined Stark effect (QCSE) originating from an out-of-plane electric field associated with the ferroelectric polarization in AlScN. 40,41 Recent reports show that excitonic complexes in monolayer TMDs can exhibit an anomalous red shift in the presence of an external electric field, owing to strong confinement resulting from their atomic scale thickness. 19,41 We speculate that the observed arresting of the blue shift in the $X_{\rm T}^{+}$ PL peak position upon cooling to 80 K is also due to the QCSE. This implies that temperature dependence of the QCSE or, equivalently, the polarization in the ferroelectric layer becomes more robust as the temperature reduces to the cryogenic temperatures leading to minimal PL peak shifts. An increase in remnant polarization at cryogenic temperatures has been reported in the past in inorganic ferroelectric materials which supports the above description on arresting of blue shift in the X_T^+ PL peak. 42,43

By fitting the broad PL spectrum with two Gaussian peaks (see Supporting Information Figure S5), we found spectral components associated with PL peak positions at ~1.64 and ~1.61 eV corresponding to positively charged bright (X_T^+) and dark trions or dark trion phonon replica (X_{DT}^{+}) , respectively. The peaks were assigned as per the previously reported and theoretically predicted binding energies in monolayer WSe_2 . 44-46 In the P_{up} polarized $WSe_2/AlScN$ FeFET device (Figure 3c), most of the temperature-dependent excitonic features remains the same, except that the broad PL emission at room temperature emerges from the negatively charged bright trions (X_T^-) , with a binding energy ~28 meV below the X° PL peak. Additionally, we observe a red shift in the PL peak at 80 K when compared to the P_{down} state device, which we again attribute to the QCSE. Furthermore, by fitting the broad PL emission, the spectral components with PL peak positions at ~1.61 and ~1.58 eV can be assigned to negatively charged

bright trions (X_T^-) and dark trions or dark trion phonon replica $(X_{\rm DT}^{-})$, with a binding energy ~26 meV below the $X_{\rm T}^{-}$ peak position, respectively (see Supporting Information Figure S6). $^{44-46}$ The asymmetric QCSE observed in the P_{down} and P_{up} states could be due to incomplete polarization switching in the P_{down} state which results in lower excess hole carrier density and lower magnitude of electric field at the WSe₂/AlScN interface in comparison to the Pup state. Also, given that WSe₂ serves as an n-type semiconducting channel even in a fully polarized P_{down} state, it is unlikely to accumulate an excess carrier density of holes to attain the same density of positively charged trions. Thus, the observed QCSE and trion effects are expected to be asymmetric. Given our experimental conditions, we also note that both singlet and triplet trions coexist in our spectra. This fine structure of trions can be better understood through the valley Zeeman effect requiring magneto-optical spectroscopy, beyond the scope of the current work.

We note that it is difficult to confirm if the ferroelectric polarization actually leads to the formation of a dark trion/dark trion phonon replica or whether this effect is purely from the red shift of the bright trion PL peak combined with significant line-width broadening. Nevertheless, these fascinating excitonic characteristics, including both bright and dark trions, can have an important impact on the valley polarization dynamics in WSe₂. It has been reported that the formation of trions can significantly influence valley polarization properties. This is because they exhibit (i) ultralong valley lifetimes compared to the neutral excitons and (ii) reduced intervalley scattering, since trions involve an extra charge (i.e., an electron-hole pair and an excess charge carrier) for simultaneous large momentum transfer and spin flip.³⁴ Moreover, their net charge can also enable detection as well as manipulation of valley currents by external electric fields. 34,44

To study the valley polarization properties of the WSe₂/ AlScN FeFET device in two oppositely polarized states, we perform polarization-resolved PL measurements excited with a right-handed, circularly polarized (σ^+) 633 nm laser and detected with right-handed (σ^+) and left-handed (σ^-) helicity to measure the emission from K and K' valleys, respectively. Figure 4a,b displays helicity-resolved PL spectra from a WSe₂/ AlScN device polarized in the $P_{\rm down}$ and $P_{\rm up}$ states at 80 K. The degree of valley polarization (DVP) was calculated using the equation $\eta = \frac{I(\sigma+) - I(\sigma-)}{I(\sigma+) + I(\sigma-)}$, where $I(\sigma+)$ and $I(\sigma-)$ refer to the right- and left-handed circular polarization resolved PL intensity, respectively.³ When the device is in the P_{down} state, X_{T}^{+} shows a very low valley polarization degree of ~4%, while in the $P_{\rm up}$ state, with increased negative charge carrier injection, the device exhibited a drastically higher DVP of ~27% in a representative WSe₂/AlScN device. This observation indicates that negatively charged trions have a greater impact on valley polarization characteristics. The evolution of valley polarization as a function of temperature is also measured and is shown in Figure 4c and Figures S7-S8 (see Supporting Information). The temperature-dependent DVP shows a gradual decrease with an increase in the temperature. This is attributed to the increase in phonon-induced intervalley scattering, leading to a change in the valley depolarization time. However, a valley polarization of ~7% still persists at room temperature. This is likely because of the large polarization of the AlScN. To demonstrate the reproducibility of the valley polarization results with ferroelectric polarization switching, we designed and measured a 3×3 array of valleytronic devices in

the $P_{\rm up}$ state (see Supporting Information Figure S9). All the devices showed enhanced valley polarization, and a maximum DVP of \sim 27% was obtained among the nine devices measured. Further, we measured retention characteristics of valley polarization in the $P_{\rm up}$ state. The measured valley polarization remains consistent up to 5400 s (90 min), implying that the ferroelectric polarization is preserved over this time scale leading to reproducible valley polarization enhancement over this time scale (Figure 4d and Figure S10 in the Supporting Information). This result holds great promise for non-volatile optoelectronic memory that encodes both electrical conductance as well as polarization of the emission. The long retention time is particularly interesting and is mainly associated with the robustness of the ferroelectric polarization state. By controlling the laser heating effect and the robustness of the ferroelectric polarization, we anticipate that the retention time can be prolonged further. Similarly, devices fabricated using MOCVD-grown, large-area WSe2 monolayers showed enhanced DVP in the P_{up} state (see Supporting Information Figures S12-S13). Very few reports describe tuning of valley polarization characteristics, especially in monolayer TMDs. To the best of our knowledge, ferroelectric tuning has never been reported. Thus, it is difficult to make a direct comparison. Nevertheless, we compare the tunability performance of our device with other tuning approaches, such as electrostatic gating and magnetic field tuning in Figure 4e. 19,20,47,48 It is evident that the ferroelectric gating approach in our device outperforms other tuning strategies. We find that valley polarization tuning of ~23% is obtained at relatively low voltages compared with electrostatic gating at higher voltages and high magnetic fields. Thus, our results indicate that ferroelectric polarization switching can be a potential knob to control valley polarization and achieve non-volatile valley addressable memory in monolayer WSe2 at comparatively low power.

The potential mechanism for the enhancement of valley polarization with ferroelectric polarization switching can be attributed to the formation of trions and strong QCSE-induced suppression of valley depolarization. For neutral excitons in monolayer TMDs, strong electron-hole (e-h) exchange interactions through the Maialle-Silva-Sham mechanism are the dominant valley depolarization process, which is relatively fast. This results in a short valley lifetime, on the order of few picoseconds, 14,15 as evidenced by the low DVP of excitons obtained in ML-WSe₂ exfoliated on the SiO₂/Si substrate (see Supporting Information Figure S14). As the density of electron or hole injection increases with ferroelectric gating, excitons in WSe2 can combine with extra charge carriers, leading to the formation of negatively or positively charged trions, respectively. For trions, valley depolarization is mainly determined by intervalley scattering, because spin and momentum are mismatched. Previous studies on graphene and other TMD systems also show that the intervalley scattering rate is significantly suppressed with increased carrier doping. 44,49 Thus, valley depolarization of trions is expected to be much slower than that observed for the excitons. As a result, trions show enhanced DVP.

To get more insight into the mechanism of valley polarization with ferroelectric gating mediated exciton to trion conversion (X-T) the following valley resolved rate equations are utilized:⁵⁰

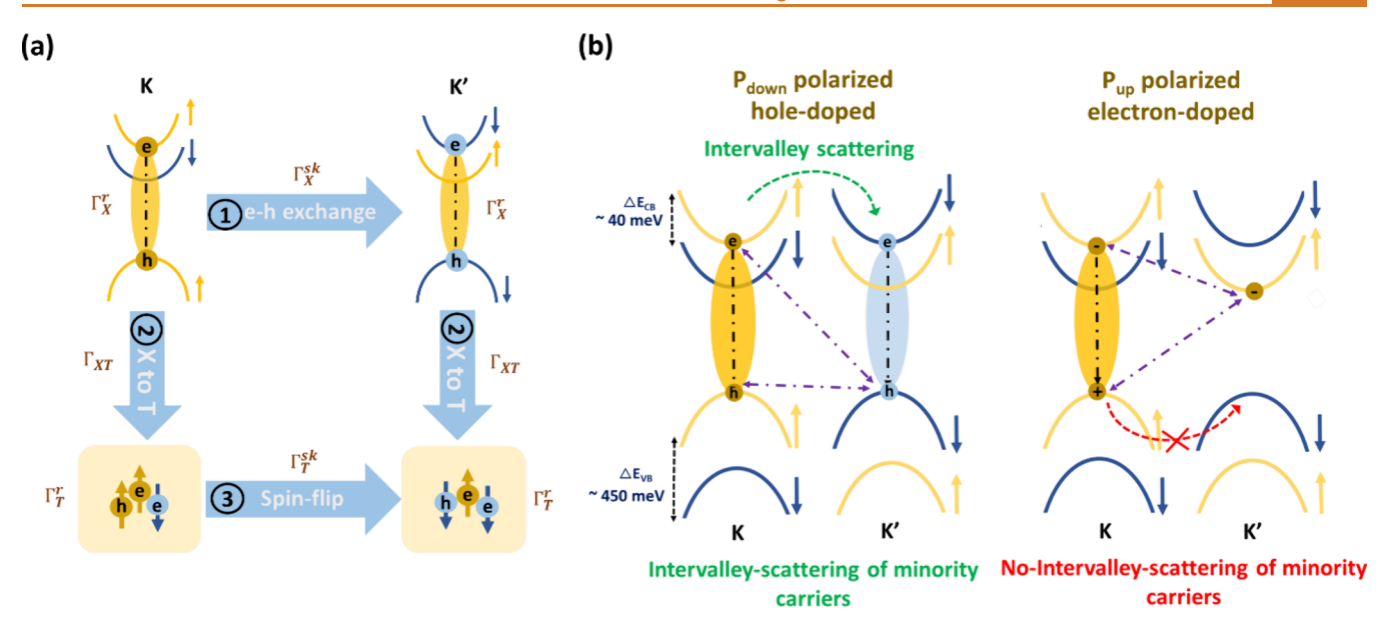


Figure 5. Valley polarization mechanism in the WSe₂/AlScN FeFET device. (a) Schematic illustration of the formation of excitons and trions and their different relaxation pathways leading to valley depolarization. (b) Intervalley scattering and valley depolarization mechanism for positively charged and negatively charged trions.

$$\frac{\mathrm{d}n_X^{K/K'}}{\mathrm{d}t} = g^{K/K'} - n_X^{K/K'} \Gamma_X^r - n_X^{K/K'} \Gamma_{XT}^r + (n_X^{K'/K} - n_X^{K/K'}) \Gamma_X^{sk}$$
(1.1)

$$\frac{\mathrm{d}n_{T}^{K/K'}}{\mathrm{d}t} = -n_{T}^{K/K'}\Gamma_{T}^{r} + n_{X}^{K/K'}\Gamma_{XT} + (n_{T}^{K'/K} - n_{T}^{K/K'})\Gamma_{T}^{sk}$$
(1.2)

here, $n_X^{K/K'}$ and $n_T^{K/K'}$ represent the density of excitons and trions in K/K' valleys; $g^{K/K'}$ is the generation rate of excitons. Γ_X^r and Γ_T^r correspond to the recombination rate of excitons and trions, and Γ_{XT} represents the exciton-to-trion (X-T) conversion rate. Γ_X^{sk} and Γ_T^{sk} represent intervalley scattering rates of excitons and trions, respectively. The solution of the above equations gives rise to DVP for excitons (η_X) and trions (η_T) , as follows:

$$\eta_X = \eta_o \frac{\Gamma_X^{ia}}{\Gamma_X^{ia} + \Gamma_X^{ir}} \tag{2.1}$$

$$\eta_T = \eta_X \frac{\Gamma_T^{ia}}{\Gamma_T^{ia} + \Gamma_T^{ir}} \tag{2.2}$$

where η_o is the initial DVP for excitons which is assumed to be 100%, Γ_X^{ia} and Γ_T^{ia} stands for the intravalley decay rate of excitons and trions, and Γ_X^{ir} and Γ_T^{ir} denote the intervalley decay rate of excitons and trions, respectively. During the process of X-T conversion, the effective intravalley decay rate for excitons and trions can be described as follows:

$$\Gamma_X^{ia} = \Gamma_X^r + \Gamma_{XT} \tag{3.1}$$

and

$$\Gamma_T^{ia} = \Gamma_T^r \tag{3.2}$$

As the probability of trion to exciton conversion reduces at low temperatures, the term Γ_{TX} is neglected in eq 3.2. For excitons, a fast decay of valley polarization is ascribed to the

faster intravalley recombination, as well as the intervalley scattering rate, which is on the order of few ps. 14,15 Since trions mainly emerge from excitons, the valley polarization for trions depends on the exciton valley polarization. For example, under σ^+ circularly polarized light excitation, trions in the K valley are formed through the excitons generated in the K valley, while the trions in the K' valley are formed either by intervalley scattering of excitons from the K to the K' valley or by spin flipping of trions formed in the K valley. The probability of spin flipping is low due to the large momentum separation between valleys, and under the condition of fast X-T conversion rate in the K valley, the formation of trions in the K' valley and the intervalley decay rate of trions are extremely low, causing an imbalance of trions in K and K' valleys which leads to enhanced DVP for the trions. The above mechanism is schematically described in Figure 5a.

It is noteworthy that, in our devices, positively and negatively charged trions exhibit an asymmetric valley polarization behavior whereby negatively charged trions exhibit an enhanced valley polarization compared to the positively charged trions (Figure 4a,b). This phenomenon can be attributed to three reasons. First, the valley lifetime of negatively charged trions is longer than positively charged trions (see Supporting Information Figure S15). 45,51-55 Second, the strong quantum confined Stark effect in the $P_{
m up}$ state compared to the $P_{\rm down}$ state leads to a higher suppression of electron-hole exchange interaction/intervalley scattering. As reported previously, the QCSE can effectively modify the overlap of electron-hole wave functions in monolayer TMDs, leading to a decrease in the intervalley scattering and spin relaxation rate. 19,56 Third, free electrons and holes possess different intervalley scattering mechanisms. For doped WSe2 samples, the electron-hole recombination, which contains the valley information, is determined mainly by the minority charge carriers, i.e., electrons in the $P_{\rm down}$ state device and holes in the $P_{\rm up}$ state device. ⁵⁵ In the $P_{\rm up}$ state device, optically excited holes determine the valley excitonic emission in WSe2 (Figure 5b), and the corresponding intervalley scattering (spinflip) time for holes is quite long due to the larger spin-splitting

at the valence band (ΔE_{VB}). Both theory and experimental studies have shown that the valley polarization lifetime of holes is on the order of nanoseconds. ^{57–59} Thus, the holes prefer to remain in the same valley as it is excited, leading to enhanced valley polarization. In the case of the P_{down} state device, the valley excitonic emission is determined by the optically excited electrons, which exhibit a very short intervalley scattering time (on the order of a few picoseconds) due to smaller spin splitting in the conduction band (ΔE_{CB}), resulting in less valley polarization. 60,61 Similar phenomena have been observed in other studies: the valley polarization is found to be suppressed in p-doped samples and enhanced in n-doped samples, and this has been attributed to a change in valley depolarization time. ^{20,40,50} Thus, we conclude that the long valley lifetime of the negatively charged trions and the strong coupling of the external electric field lead to enhanced valley polarization in our P_{up} polarized WSe₂/AlScN device.

CONCLUSIONS

In summary, we demonstrate a potential approach that uses ferroelectric materials to control valley polarization in monolayer TMDs. We show that the anticipated non-volatile electrical control of valley polarization could be realized experimentally by coupling a WSe $_2$ monolayer to a high $P_{\rm r}$ ferroelectric such as AlScN. Enhanced, non-volatile valley polarization, robust even at room temperature, was demonstrated by controlling the polarization state of the AlScN. This approach will allow the control and manipulation of excited state and valley polarized phenomena in 2D and other quantum materials using ground-state ferroelectric polarization control. In principle, this largely unexplored aspect within heterostructure systems has the potential to develop future ferrovalleytronic devices and sensors.

METHODS AND EXPERIMENTAL SECTION

Sample Preparation and Device Fabrication. Mechanical Exfoliation of μ m-Scale Monolayer WSe₂. WSe₂ monolayers were mechanically exfoliated from commercial bulk crystals (purchased from hq graphene, Inc.) and transferred onto AlScN by the drytransfer method. The sample preparation process was carried out inside the glovebox to avoid any sample degradation.

Large Area Mechanical Exfoliation and Transfer of Monolayer WSe₂. Large area WSe₂ was exfoliated using gold tape by following procedures in a previous study. ⁶² Gold tape was prepared by spin coating a polyvinylpyrrolidone (PVP) film on a 150 nm gold film on a SiO₂/Si substrate and then releasing the PVP/gold film by thermal release tape. A released gold surface is attached to a freshly cleaved WSe₂ bulk crystal (HQ graphene) to produce a large area monolayer. An exfoliated monolayer was transferred onto an AlScN substrate.

Synthesis of WSe₂ Monolayer by MOCVD. The growth of monolayer WSe2 on 2 in. diameter c-plane sapphire was carried out in a metal-organic chemical vapor deposition (MOCVD) system equipped with a cold-wall horizontal reactor with an inductively heated graphite susceptor with gas-foil wafer rotation.⁶³ Tungsten hexacarbonyl (W(CO)₆) was used as the metal precursor while hydrogen selenide (H₂Se) was the chalcogen source with H₂ as the carrier gas. The W(CO)₆ powder was maintained at 30 °C and 400 Torr in a stainless-steel bubbler. The synthesis of monolayer WSe2 is based on a multistep process, consisting of nucleation, ripening, and lateral growth steps, which was described previously.⁶⁴ In general, the WSe₂ sample was nucleated for 30 s at 850 °C, then ripened for 5 min at 850 °C and 5 min at 1000 °C, and then grown for 20 min at 1000 °C, which gives rise to a coalesced monolayer WSe₂ across the entire 2 in. wafer. During the lateral growth, the tungsten flow rate was set as 3.8×10^{-3} sccm and the chalcogen flow rate was set as 75 sccm while the reactor pressure was kept at 200 Torr. After growth, the substrate

was cooled in H_2Se to 300 °C to inhibit decomposition of the obtained monolayer WSe₂ film.

Deposition of AlScN Thin Film. The depositions of 45 nm AlScN were performed on 4 in. Pt(111)/Ti/SiO $_2$ /Si wafers via 150 kHz pulsed DC cosputtering with 20 s.c.c.m. N $_2$ flow under 8.3 \times 10⁻⁴ mbar in an Evatec CLUSTERLINE 200 II pulsed d.c. sputtering system. The chamber temperature was maintained at 350 °C. The growth conditions are similar to those used in our prior report of FeFETs. ³²

Device Fabrication. The large-area exfoliated and MOCVD grown monolayer WSe₂ having a size of around mm² to cm² scale was transferred on a 1 cm²-size AlScN wafer using the method explained above. Then, the WSe₂ exfoliated sample was coated using "PMMA A4 and PMMA A8" followed by source/drain (S/D) patterning via electron beam lithography (EBL). After developing the sample using Methyl Iso-Butyl Ketone (MIBK), a Ti/Au 10 nm/50 nm layer was deposited using electron beam evaporation. Then, to lift-off the deposited metal, the sample was soaked in acetone for about 20 min, gently shaken, and then rinsed with IPA. Next, to define the channel area, a second patterning using EBL was done after coating the same PMMA resists, followed by developing via MIBK. Finally, the WSe₂ in the exposed area was etched using oxygen reactive ion etching (RIE).

Characterizations. Electrical Measurement of the WSe₂/AlScN FeFET. Electrical measurements were performed using the Lakeshore probe station using a Keithley 4200A semiconductor characterization system in air at room temperature. The SMU connection was used to obtain the DC I-V characteristics. The drain current was recorded with a 0.2 V step. For polarization switching of the AlScN, the gate voltage of +10 or -10 V was applied while the source is grounded.

TEM/STEM Sample Preparation and Measurements. STEM/TEM cross-sectional samples of the devices were prepared by a plasma-focused ion beam (TESCAN S8000X PFIB-SEM) system using the in situ lift-out technique. The sample was coated with electron beam and ion beam deposition of Pt protection layers to prevent charging and heating effects (to prevent damaging monolayer 2D material) during FIB milling. The final thinning with FIB was performed at 10 kV with 20 pA current to achieve an $\sim 50 \pm 5$ nm sample thickness. TEM characterization and image acquisition were carried out on a JEOL F200 and a JEOL NEOARM operated at a 200 kV accelerating voltage. The sample was orientated to the [001] zone axis for imaging. All of the captured TEM images were collected using Digital Micrograph software (DM, Gatan Inc., USA).

Atomic Force Microscopy. The layer thickness of the WSe₂ monolayer transferred on AlScN substrate was determined using Omega Scope Smart SPM (AIST) atomic force microscopy.

Optical Measurements. Microphotoluminescence measurements were performed using a Horiba LabRam HR Evolution confocal microscope. A 633 nm continuous wave laser was used as the excitation source. Temperature-dependent PL measurements in the temperature range of 80-295 K with a cooling/heating rate of ~5 °C/min were performed using a liquid nitrogen cryostat. During the measurements, the samples were kept in a Linkam stage under a vacuum level of $\sim 10^{-3}$ Torr. A 50× objective with NA ~ 0.9 was used for the sample excitation, and the signal was collected by the same objective and electron multiplying charge coupled detector. For the circular polarization resolved PL measurements, a quarter wave plate was used to convert linearly polarized excitation light into circularly polarized light, which was subsequently focused onto the sample. The signal is collected by the same quarter-wave plate. The right-hand (σ^{+}) and left-hand (σ^{-}) polarized PL signals are consequently converted to linear polarization and selectively detected using a linear polarizer. Based on our experience in performing circularly polarized PL spectroscopy measurements on various valleytronic devices, we estimated a 0.5% error in measuring valley polarization values by using our confocal microscopy system.

ASSOCIATED CONTENT

Supporting Information

The Supporting Information is available free of charge at https://pubs.acs.org/doi/10.1021/acsnano.4c04684.

Additional optical and PL mapping images of FeFET devices, AFM image and Raman spectra of monolayer WSe₂ (mechanically exfoliated and MOCVD grown), additional PL intensity maps and low temperature PL spectra from devices in the downward and upward polarized states, temperature-dependent helicity resolved PL measurements from mechanically exfoliated WSe₂/ AlScN FeFET devices, helicity resolved PL measurements from a large area 3 × 3 array of devices, timedependent helicity resolved PL measurements from a representative FeFET device, additional I-V characteristics of WSe2/AlScN FeFET devices, helicity resolved PL measurements from FeFET devices fabricated using MOCVD grown monolayer WSe₂ and WSe₂/SiO₂/Si devices, and schematic representation of different excitonic complexes and with their respective valley depolarization time scales (PDF)

AUTHOR INFORMATION

Corresponding Author

Deep Jariwala — Department of Electrical and Systems Engineering, University of Pennsylvania, Philadelphia, Pennsylvania 19104, United States; oorcid.org/0000-0002-3570-8768; Email: dmj@seas.upenn.edu

Authors

Simrjit Singh — Department of Electrical and Systems Engineering, University of Pennsylvania, Philadelphia, Pennsylvania 19104, United States; Department of Applied Physics and Science Education, Eindhoven University of Technology, Eindhoven 5600 MB, The Netherlands

Kwan-Ho Kim – Department of Electrical and Systems Engineering, University of Pennsylvania, Philadelphia, Pennsylvania 19104, United States

Kiyoung Jo — Department of Electrical and Systems Engineering, University of Pennsylvania, Philadelphia, Pennsylvania 19104, United States; orcid.org/0000-0003-4587-234X

Pariasadat Musavigharavi — Department of Electrical and Systems Engineering and Department of Materials Science and Engineering, University of Pennsylvania, Philadelphia, Pennsylvania 19104, United States; Department of Materials Science and Engineering, University of Central Florida, Orlando, Florida 32816, United States; orcid.org/0000-0002-2977-5868

Bumho Kim – Department of Physics and Astronomy, University of Pennsylvania, Philadelphia, Pennsylvania 19104, United States; © orcid.org/0000-0002-5671-5641

Jeffrey Zheng — Department of Materials Science and Engineering, University of Pennsylvania, Philadelphia, Pennsylvania 19104, United States

Nicholas Trainor – Department of Materials Science and Engineering, Pennsylvania State University, University Park, Pennsylvania 16801, United States

Chen Chen – 2D Crystal Consortium Materials Innovation Platform, Materials Research Institute, Pennsylvania State University, University Park, Pennsylvania 16801, United States Joan M. Redwing — Department of Materials Science and Engineering and 2D Crystal Consortium Materials Innovation Platform, Materials Research Institute, Pennsylvania State University, University Park, Pennsylvania 16801, United States; orcid.org/0000-0002-7906-452X

Eric A. Stach — Department of Materials Science and Engineering, University of Pennsylvania, Philadelphia, Pennsylvania 19104, United States; orcid.org/0000-0002-3366-2153

Roy H. Olsson, III – Department of Electrical and Systems Engineering, University of Pennsylvania, Philadelphia, Pennsylvania 19104, United States

Complete contact information is available at: https://pubs.acs.org/10.1021/acsnano.4c04684

Author Contributions

S.S. and D.J. conceived the idea and designed the experiments. S.S. carried out the small area mechanical exfoliation, and B.K. carried out large area mechanical exfoliation of monolayer WSe₂ on AlScN, respectively. N.T. and C.C. prepared wafer scale monolayer WSe₂ using MOCVD under the supervision of J.M.R. K.-H.K. fabricated valleytronic devices from the exfoliated and MOCVD grown samples and measured *I–V* characteristics. P.M. carried out TEM/STEM measurements under the supervision of E.A.S. J.Z. performed sputtering of AlScN films under the supervision of R.H.O. S.S. performed photoluminescence spectroscopy, circularly polarized PL, AFM, and Raman spectroscopy measurements with the help of K.J. S.S. analyzed the data by discussion with all authors. S.S. and D.J wrote the paper. All authors discussed the results and commented on the manuscript.

Notes

The authors declare no competing financial interest.

ACKNOWLEDGMENTS

D.J. and K-H.K. acknowledge primary funding support by the Air Force Office of Scientific Research (AFOSR) GHz-THz core program FA9550-23-1-0391. S.S. acknowledges support from the Fulbright-Nehru fellowship by United States-India Education Foundation (USIEF). S.S. also acknowledges partial support from the European Union's Horizon 2020 research and innovation program under the Marie Skłodowska-Curie grant agreement No. 899987. D.J. and K.J. acknowledge partial support from the Asian Office of Aerospace Research and Development (AOARD) of the AFOSR FA2386-20-1-4074 and FA2386-21-1-4063. K.J. acknowledges partial support from the Vagelos Institute of Energy Science and Technology Graduate Fellowship. Work by B.K. is supported by the U.S. Office of Naval Research (ONR) through grant N00014-20-1-2325 on Robust Photonic Materials with High-Order Topological Protection. R.H.O. acknowledges support from the NSF CAREER Award (1944248). N.T. acknowledges support from the National Science Foundation Graduate Research Fellowship Program under Grant No. DGE1255832. The MOCVD WSe₂ samples were provided by the 2D Crystal Consortium Materials Innovation Platform (2DCC-MIP) facility at Penn State which is funded by NSF under cooperative agreement DMR-2039351. Microfabrication and electron microscopy were performed at the Singh Center for Nanotechnology, supported by the NSF National Nanotechnology Coordinated Infrastructure Program (NNCI-1542153). The authors acknowledge the use of facilities and

instrumentation supported by NSF University of Pennsylvania Materials Research Science and Engineering Center (MRSEC) (DMR-1720530 and 2309043).

REFERENCES

- (1) Vitale, S. A.; Nezich, D.; Varghese, J. O.; Kim, P.; Gedik, N.; Jarillo-Herrero, P.; Xiao, D.; Rothschild, M. Valleytronics: Opportunities, Challenges, and Paths Forward. *Small.* **2018**, *14* (38), 1801483.
- (2) Schaibley, J. R.; Yu, H.; Clark, G.; Rivera, P.; Ross, J. S.; Seyler, K. L.; Yao, W.; Xu, X. Valleytronics in 2D Materials. *Nat. Rev. Mater.* **2016**, *1*, 16055.
- (3) Zhao, S.; Li, X.; Dong, B.; Wang, H.; Wang, H.; Zhang, Y.; Han, Z.; Zhang, H. Valley Manipulation in Monolayer Transition Metal Dichalcogenides and Their Hybrid Systems: Status and Challenges. *Rep. Prog. Phys.* **2021**, *84*, 026401.
- (4) Zeng, H.; Dai, J.; Yao, W.; Xiao, D.; Cui, X. Valley Polarization in MoS 2 Monolayers by Optical Pumping. *Nat. Nanotechnol* **2012**, 7 (8), 490–493.
- (5) Eginligil, M.; Cao, B.; Wang, Z.; Shen, X.; Cong, C.; Shang, J.; Soci, C.; Yu, T. Dichroic Spin-Valley Photocurrent in Monolayer Molybdenum Disulphide. *Nat. Commun.* **2015**, *6*, 7636.
- (6) Aas, S.; Bulutay, C. Strain Dependence of Photoluminescence and Circular Dichroism in Transition Metal Dichalcogenides: A k · p Analysis. *Opt Express* **2018**, *26* (22), 28672.
- (7) Sie, E. J.; Lui, C. H.; Lee, Y. H.; Kong, J.; Gedik, N. Observation of Intervalley Biexcitonic Optical Stark Effect in Monolayer WS2. *Nano Lett.* **2016**, *16* (12), 7421–7426.
- (8) Cunningham, P. D.; Hanbicki, A. T.; Reinecke, T. L.; McCreary, K. M.; Jonker, B. T. Resonant Optical Stark Effect in Monolayer WS2. *Nat. Commun.* **2019**, *10* (1), 5539.
- (9) LaMountain, T.; Nelson, J.; Lenferink, E. J.; Amsterdam, S. H.; Murthy, A. A.; Zeng, H.; Marks, T. J.; Dravid, V. P.; Hersam, M. C.; Stern, N. P. Valley-Selective Optical Stark Effect of Exciton-Polaritons in a Monolayer Semiconductor. *Nat. Commun.* **2021**, *12* (1), 4530.
- (10) Onga, M.; Zhang, Y.; Ideue, T.; Iwasa, Y. Exciton Hall Effect in Monolayer MoS 2. *Nat. Mater.* **2017**, *16* (12), 1193–1197.
- (11) Huang, Z.; Liu, Y.; Dini, K.; Tan, Q.; Liu, Z.; Fang, H.; Liu, J.; Liew, T.; Gao, W. Robust Room Temperature Valley Hall Effect of Interlayer Excitons. *Nano Lett.* **2020**, *20* (2), 1345–1351.
- (12) Wu, Y. J.; Shen, C.; Tan, Q. H.; Shi, J.; Liu, X. F.; Wu, Z. H.; Zhang, J.; Tan, P. H.; Zheng, H. Z. Valley Zeeman Splitting of Monolayer MoS2 Probed by Low-Field Magnetic Circular Dichroism Spectroscopy at Room Temperature. *Appl. Phys. Lett.* **2018**, *112* (15), 153105.
- (13) Norden, T.; Zhao, C.; Zhang, P.; Sabirianov, R.; Petrou, A.; Zeng, H. Giant Valley Splitting in Monolayer WS2 by Magnetic Proximity Effect. *Nat. Commun.* **2019**, *10* (1), 4163.
- (14) Wu, Y. C.; Taniguchi, T.; Watanabe, K.; Yan, J. Enhancement of Exciton Valley Polarization in Monolayer Induced by Scattering. *Phys. Rev. B* **2021**, *104* (12), L121408.
- (15) Xu, S.; Si, C.; Li, Y.; Gu, B. L.; Duan, W. Valley Depolarization Dynamics in Monolayer Transition-Metal Dichalcogenides: Role of the Satellite Valley. *Nano Lett.* **2021**, *21* (4), 1785–1791.
- (16) Srivastava, A.; Sidler, M.; Allain, A. V.; Lembke, D. S.; Kis, A.; Imamoğlu, A. Valley Zeeman Effect in Elementary Optical Excitations of Monolayer WSe 2. *Nat. Phys.* **2015**, *11* (2), 141–147.
- (17) Macneill, D.; Heikes, C.; Mak, K. F.; Anderson, Z.; Kormányos, A.; Zólyomi, V.; Park, J.; Ralph, D. C. Breaking of Valley Degeneracy by Magnetic Field in Monolayer MoSe2. *Phys. Rev. Lett.* **2015**, *114* (3), 037401.
- (18) Aivazian, G.; Gong, Z.; Jones, A. M.; Chu, R. L.; Yan, J.; Mandrus, D. G.; Zhang, C.; Cobden, D.; Yao, W.; Xu, X. Magnetic Control of Valley Pseudospin in Monolayer WSe 2. *Nat. Phys.* **2015**, *11* (2), 148–152.
- (19) Chakraborty, C.; Mukherjee, A.; Qiu, L.; Vamivakas, A. N. Electrically Tunable Valley Polarization and Valley Coherence in

- Monolayer WSe 2 Embedded in a van Der Waals Heterostructure. Opt Mater. Express 2019, 9 (3), 1479.
- (20) Feng, S.; Cong, C.; Konabe, S.; Zhang, J.; Shang, J.; Chen, Y.; Zou, C.; Cao, B.; Wu, L.; Peimyoo, N.; Zhang, B.; Yu, T. Engineering Valley Polarization of Monolayer WS 2: A Physical Doping Approach. *Small* **2019**, *15* (12), 1805503.
- (21) Shinokita, K.; Wang, X.; Miyauchi, Y.; Watanabe, K.; Taniguchi, T.; Matsuda, K. Continuous Control and Enhancement of Excitonic Valley Polarization in Monolayer WSe₂ by Electrostatic Doping. *Adv. Funct Mater.* **2019**, 29 (26), 1900260.
- (22) Mikolajick, T.; Slesazeck, S.; Mulaosmanovic, H.; Park, M. H.; Fichtner, S.; Lomenzo, P. D.; Hoffmann, M.; Schroeder, U. Next Generation Ferroelectric Materials for Semiconductor Process Integration and Their Applications. J. Appl. Phys. 2021, 129 (10), 100901.
- (23) Pei, Q.; Mi, W. Electrical Control of Magnetic Behavior and Valley Polarization of Monolayer Antiferromagnetic Mn PSe3 on an Insulating Ferroelectric Substrate from First Principles. *Phys. Rev. Appl.* **2019**, *11* (1), 014011.
- (24) Hu, H.; Tong, W. Y.; Shen, Y. H.; Duan, C. G. Electrical Control of the Valley Degree of Freedom in 2D Ferroelectric/Antiferromagnetic Heterostructures. *J. Mater. Chem. C Mater.* **2020**, 8 (24), 8098–8106.
- (25) Lei, C.; Xu, X.; Zhang, T.; Huang, B.; Dai, Y.; Ma, Y. Nonvolatile Controlling Valleytronics by Ferroelectricity in 2H-VSe2/Sc2CO2van Der Waals Heterostructure. *J. Phys. Chem. C* **2021**, *125* (4), 2802–2809.
- (26) Kim, J. Y.; Choi, M. J.; Jang, H. W. Ferroelectric Field Effect Transistors: Progress and Perspective. *APL Mater.* **2021**, 9 (2), 02.1102.
- (27) Institute of Electrical and Electronics Engineers. *IEEE 11th International Memory Workshop: IMW 2019*, 12–15 May 2019, Monterey, California, USA.
- (28) Mikolajick, T.; Schroeder, U.; Slesazeck, S. Hafnium Oxide Based Ferroelectric Devices for Memories and Beyond. In 2018 International Symposium on VLSI Technology, Systems and Application, VLSI-TSA 2018; Institute of Electrical and Electronics Engineers Inc., 2018; pp 1–2; DOI: 10.1109/VLSI-TSA.2018.8403848.
- (29) Rodriguez, J. R.; Murray, W.; Fujisawa, K.; Lee, S. H.; Kotrick, A. L.; Chen, Y.; McKee, N.; Lee, S.; Terrones, M.; Trolier-Mckinstry, S.; Jackson, T. N.; Mao, Z.; Liu, Z.; Liu, Y. Electric Field Induced Metallic Behavior in Thin Crystals of Ferroelectric α -In2Se3. *Appl. Phys. Lett.* **2020**, *117* (5), 052901.
- (30) Li, Y.; Gong, M.; Zeng, H. Atomically Thin In2Se3: An Emergent Two-Dimensional Room Temperature Ferroelectric Semiconductor. *Journal of Semiconductors* **2019**, *40*, 061002.
- (31) Chiang, C. K.; Popielarz, R. Polymer Composites with High Dielectric Constant. *Ferroelectrics* **2002**, *275*, 1–9.
- (32) Kim, K.-H.; Song, S.; Kim, B.; Musavigharavi, P.; Trainor, N.; Katti, K.; Chen, C.; Kumari, S.; Zheng, J.; Redwing, J. M.; Stach, E. A.; Olsson, R. H., III; Jariwala, D. Tuning Polarity in WSe₂/AlScN FeFETs via Contact Engineering. *ACS Nano* **2024**, *18* (5), 4180–4188.
- (33) Liu, E.; Van Baren, J.; Liang, C. T.; Taniguchi, T.; Watanabe, K.; Gabor, N. M.; Chang, Y. C.; Lui, C. H. Multipath Optical Recombination of Intervalley Dark Excitons and Trions in Monolayer WSe2. *Phys. Rev. Lett.* **2020**, *124* (19), 196802.
- (34) Fu, J.; Cruz, J. M. R.; Qu, F. Valley Dynamics of Different Trion Species in Monolayer WSe2. *Appl. Phys. Lett.* **2019**, *115* (8), 082101.
- (35) Li, C. H.; McCreary, K. M.; Jonker, B. T. Spatial Control of Photoluminescence at Room Temperature by Ferroelectric Domains in Monolayer WS2/PZT Hybrid Structures. *ACS Omega* **2016**, *1* (6), 1075–1080.
- (36) Jadczak, J.; Kutrowska-Girzycka, J.; Kapuściński, P.; Huang, Y. S.; Wójs, A.; Bryja, L. Probing of Free and Localized Excitons and Trions in Atomically Thin WSe2, WS2, MoSe2 and MoS2 in Photoluminescence and Reflectivity Experiments. *Nanotechnology* **2017**, 28 (39), 395702.

- (37) Kunstmann, J.; Mooshammer, F.; Nagler, P.; Chaves, A.; Stein, F.; Paradiso, N.; Plechinger, G.; Strunk, C.; Schüller, C.; Seifert, G.; Reichman, D. R.; Korn, T. Momentum-Space Indirect Interlayer Excitons in Transition-Metal Dichalcogenide van Der Waals Heterostructures. *Nat. Phys.* **2018**, *14*, 801–805.
- (38) Wang, G.; Bouet, L.; Lagarde, D.; Vidal, M.; Balocchi, A.; Amand, T.; Marie, X.; Urbaszek, B. Valley Dynamics Probed through Charged and Neutral Exciton Emission in Monolayer WSe2. *Phys. Rev. B Condens Matter Mater. Phys.* **2014**, 90 (7), 075413.
- (39) Yan, T.; Qiao, X.; Liu, X.; Tan, P.; Zhang, X. Photoluminescence Properties and Exciton Dynamics in Monolayer WSe 2. *Appl. Phys. Lett.* **2014**, *105* (10), 101901.
- (40) Jones, A. M.; Yu, H.; Ghimire, N. J.; Wu, S.; Aivazian, G.; Ross, J. S.; Zhao, B.; Yan, J.; Mandrus, D. G.; Xiao, D.; Yao, W.; Xu, X. Optical Generation of Excitonic Valley Coherence in Monolayer WSe 2. Nat. Nanotechnol 2013, 8 (9), 634–638.
- (41) Abraham, N.; Watanabe, K.; Taniguchi, T.; Majumdar, K. Anomalous Stark Shift of Excitonic Complexes in Monolayer WS2. *Phys. Rev. B* **2021**, *103* (7), 075430.
- (42) Crawford, J. C. Ferroelectric Field Effect Studies at Low Temperatures. *Ferroelectrics* **1970**, *1* (1), 23–30.
- (43) Meng, X. J.; Sun, J. L.; Wang, X. G.; Lin, T.; Ma, J. H.; Guo, S. L.; Chu, J. H. Temperature Dependence of Ferroelectric and Dielectric Properties of PbZr0.5Ti0.5O3 Thin Film Based Capacitors. *Appl. Phys. Lett.* **2002**, *81* (21), 4035–4037.
- (44) Liu, E.; Van Baren, J.; Lu, Z.; Altaiary, M. M.; Taniguchi, T.; Watanabe, K.; Smirnov, D.; Lui, C. H. Gate Tunable Dark Trions in Monolayer WSe2. *Phys. Rev. Lett.* **2019**, *123* (2), 027401.
- (45) Yang, M.; Ren, L.; Robert, C.; Van Tuan, D.; Lombez, L.; Urbaszek, B.; Marie, X.; Dery, H. Relaxation and Darkening of Excitonic Complexes in Electrostatically Doped Monolayer Formula Presented: Roles of Exciton-Electron and Trion-Electron Interactions. *Phys. Rev. B* **2022**, *105* (8), 085302.
- (46) Courtade, E.; Semina, M.; Manca, M.; Glazov, M. M.; Robert, C.; Cadiz, F.; Wang, G.; Taniguchi, T.; Watanabe, K.; Pierre, M.; Escoffier, W.; Ivchenko, E. L.; Renucci, P.; Marie, X.; Amand, T.; Urbaszek, B. Charged Excitons in Monolayer WSe2: Experiment and Theory. *Phys. Rev. B* **2017**, *96* (8), 085302.
- (47) Aivazian, G.; Gong, Z.; Jones, A. M.; Chu, R. L.; Yan, J.; Mandrus, D. G.; Zhang, C.; Cobden, D.; Yao, W.; Xu, X. Magnetic Control of Valley Pseudospin in Monolayer WSe 2. *Nat. Phys.* **2015**, *11* (2), 148–152.
- (48) Plechinger, G.; Nagler, P.; Arora, A.; Granados Del Águila, A.; Ballottin, M. V.; Frank, T.; Steinleitner, P.; Gmitra, M.; Fabian, J.; Christianen, P. C. M.; Bratschitsch, R.; Schüller, C.; Korn, T. Excitonic Valley Effects in Monolayer WS2 under High Magnetic Fields. *Nano Lett.* **2016**, *16* (12), 7899–7904.
- (49) Yan, B.; Han, Q.; Jia, Z.; Niu, J.; Cai, T.; Yu, D.; Wu, X. Electrical Control of Intervalley Scattering in Graphene via the Charge State of Defects. *Phys. Rev. B* **2016**, 93 (4), 041407.
- (50) Zhang, Q.; Sun, H.; Tang, J.; Dai, X.; Wang, Z.; Ning, C. Z. Prolonging Valley Polarization Lifetime through Gate-Controlled Exciton-to-Trion Conversion in Monolayer Molybdenum Ditelluride. *Nat. Commun.* **2022**, *13* (1), 4101.
- (51) Ersfeld, M.; Volmer, F.; Rathmann, L.; Kotewitz, L.; Heithoff, M.; Lohmann, M.; Yang, B.; Watanabe, K.; Taniguchi, T.; Bartels, L.; Shi, J.; Stampfer, C.; Beschoten, B. Unveiling Valley Lifetimes of Free Charge Carriers in Monolayer WSe2. *Nano Lett.* **2020**, *20* (5), 3147–3154.
- (52) Yang, L.; Sinitsyn, N. A.; Chen, W.; Yuan, J.; Zhang, J.; Lou, J.; Crooker, S. A. Long-Lived Nanosecond Spin Relaxation and Spin Coherence of Electrons in Monolayer MoS 2 and WS 2. *Nat. Phys.* **2015**, *11* (10), 830–834.
- (53) Yang, L.; Chen, W.; McCreary, K. M.; Jonker, B. T.; Lou, J.; Crooker, S. A. Spin Coherence and Dephasing of Localized Electrons in Monolayer MoS2. *Nano Lett.* **2015**, *15* (12), 8250–8254.
- (54) McCormick, E. J.; Newburger, M. J.; Luo, Y. K.; McCreary, K. M.; Singh, S.; Martin, I. B.; Cichewicz, E. J.; Jonker, B. T.; Kawakami,

- R. K. Imaging Spin Dynamics in Monolayer WS2 by Time-Resolved Kerr Rotation Microscopy. 2d Mater. 2018, 5 (1), 011010.
- (55) Li, Z.; Wang, T.; Lu, Z.; Khatoniar, M.; Lian, Z.; Meng, Y.; Blei, M.; Taniguchi, T.; Watanabe, K.; McGill, S. A.; Tongay, S.; Menon, V. M.; Smirnov, D.; Shi, S. F. Direct Observation of Gate-Tunable Dark Trions in Monolayer WSe2. *Nano Lett.* **2019**, *19* (10), 6886–6802
- (56) Abraham, N.; Watanabe, K.; Taniguchi, T.; Majumdar, K. Anomalous Stark Shift of Excitonic Complexes in Monolayer WS2. *Phys. Rev. B* **2021**, *103* (7), 075430.
- (57) Song, X.; Xie, S.; Kang, K.; Park, J.; Sih, V. Long-Lived Hole Spin/Valley Polarization Probed by Kerr Rotation in Monolayer WSe2. *Nano Lett.* **2016**, *16* (8), 5010–5014.
- (58) Mak, K. F.; He, K.; Shan, J.; Heinz, T. F. Control of Valley Polarization in Monolayer MoS2 by Optical Helicity. *Nat. Nanotechnol* **2012**, *7* (8), 494–498.
- (59) Ochoa, H.; Roldán, R. Spin-Orbit-Mediated Spin Relaxation in Monolayer MoS2. *Phys. Rev. B Condens Matter Mater. Phys.* **2013**, 87 (24), 245421.
- (60) Plechinger, G.; Nagler, P.; Schüller; Korn, T. Time-Resolved Kerr Rotation Spectroscopy of Valley Dynamics in Single-Layer MoS₂. arXiv **2014**, 1404.7674.
- (61) Dal Conte, S.; Bottegoni, F.; Pogna, E. A. A.; Ambrogio, S.; Bargigia, I.; D'Andrea, C.; De Fazio, D.; Lombardo, A.; Bruna, M.; Ciccacci, F.; Ferrari, A. C.; Cerullo, G.; Finazzi, M. Valley and Spin Dynamics in Monolayer MoS₂. *arXiv* **2015**, 1502.06817.
- (62) Liu, F.; Wu, W.; Bai, Y.; Chae, S. H.; Li, Q.; Wang, J.; Hone, J.; Zhu, X.-Y. Disassembling 2D van Der Waals Crystals into Macroscopic Monolayers and Reassembling into Artificial Lattices. *Science* **2020**, 367, 903–906.
- (63) Xuan, Y.; Jain, A.; Zafar, S.; Lotfi, R.; Nayir, N.; Wang, Y.; Choudhury, T. H.; Wright, S.; Feraca, J.; Rosenbaum, L.; Redwing, J. M.; Crespi, V.; van Duin, A. C. T. Multi-Scale Modeling of Gas-Phase Reactions in Metal-Organic Chemical Vapor Deposition Growth of WSe2. *J. Cryst. Growth* **2019**, *527*, 125247.
- (64) Zhang, X.; Choudhury, T. H.; Chubarov, M.; Xiang, Y.; Jariwala, B.; Zhang, F.; Alem, N.; Wang, G. C.; Robinson, J. A.; Redwing, J. M. Diffusion-Controlled Epitaxy of Large Area Coalesced WSe2Monolayers on Sapphire. *Nano Lett.* **2018**, *18* (2), 1049–1056.